Direct Visualization of Exciton Reequilibration in the LH1 and LH2 Complexes of *Rhodobacter sphaeroides* by Multipulse Spectroscopy

Thomas A. Cohen Stuart,[†*] Mikas Vengris,[‡] Vladimir I. Novoderezhkin,[§] Richard J. Cogdell,[¶] C. Neil Hunter,[‖] and Rienk van Grondelle[†]

[†]Faculty of Sciences, Free University of Amsterdam, de Boelelaan, Amsterdam, The Netherlands; [‡]Vilnius University, Faculty of Physics, Quantum Electronics Department, Vilnius, Lithuania; [§]A.N. Belozersky Institute of Physico-Chemical Biology, Moscow State University, Moscow, Russia; [¶]Microbial Photosynthesis Laboratory, Glasgow Biomedical Research Centre, University of Glasgow, Glasgow, United Kingdom; and [‖]Department of Molecular Biology and Biotechnology, University of Sheffield, Sheffield, United Kingdom

ABSTRACT The dynamics of the excited states of the light-harvesting complexes LH1 and LH2 of *Rhodobacter sphaeroides* are governed, mainly, by the excitonic nature of these ring-systems. In a pump-dump-probe experiment, the first pulse promotes LH1 or LH2 to its excited state and the second pulse dumps a portion of the excited state. By selective dumping, we can disentangle the dynamics normally hidden in the excited-state manifold. We find that by using this multiple-excitation technique we can visualize a 400-fs reequilibration reflecting relaxation between the two lowest exciton states that cannot be directly explored by conventional pump-probe. An oscillatory feature is observed within the exciton reequilibration, which is attributed to a coherent motion of a vibrational wavepacket with a period of ~150 fs. Our disordered exciton model allows a quantitative interpretation of the observed reequilibration processes occurring in these antennas.

INTRODUCTION

In photosynthetic purple bacteria, antenna pigment proteins residing in the intracytoplasmic cell membrane absorb solar light and transport the energy to the bacterial reaction center (RC), where the light energy is converted into utilizable chemical energy (1–3). These antenna molecules are referred to as Light Harvesting complex 1 (LH1) and Light Harvesting complex 2 (LH2). The LH1 core antenna, a closely coupled pigment system, surrounds the bacterial reaction center (4,5). LH1 is, in many types of bacteria, connected to a peripheral antenna, LH2 (6). The elementary building block of both LH1 and LH2 is a coupled pair of helical transmembrane polypeptides, composing the so-called α/β dimer. Both helices bind a bacteriochlorophyll a (BChl a) at a conserved histidine position (7), and in the case of LH2, the β-polypeptide also binds a second *BChl a* (6,8). The α/β dimers are arranged in ringlike structures. In the case of the LH1 complex of *Rhodobacter* (*Rba.*) *sphaeroides*, the BChls form two interconnected open rings of 28 dimers in total, with each dimer proposed to have a gate for quinone exchange formed by the PufX protein (9–13). In the case of LH2, there is a circular arrangement of 9 α/β dimers binding two concentric rings of 18 B850 BChls and 9 B800 BChls, structurally and energetically connected by carotenoid molecules (14). The major interactions that stabilize LH1 are, in fact, within the α/β subunits.

In contrast, in LH2, amino acids of neighboring interactions between α/β-pairs are essential (6,15). These rings are named according to their absorption maxima, B875 (LH1), B850 (LH2), and B800 (LH2). A wide variety of one-dimensional spectroscopic techniques has been employed specifically to uncover the early dynamics happening in the excited-state manifold of LH1 and LH2 in relation to their spectroscopic properties (14,16–24). A biphasic equilibration of exciton states with lifetimes of ~100 fs and ~400 fs is generally reported. Experiments with short laser pulses also revealed faster (10–100 fs) components (16,25–28). Interaction energies between the BChls of these rings are estimated to be at ~250–450 cm^{-1} for LH2 and 400–600 cm^{-1} in LH1 (19,29–31).

Extensive calculation done by Tretiak et al. (32) and Krueger et al. (33) verified the interaction energies and disorder coupling parameters reported for the BChls in LH2. An indication of the involvement of the collective exciton states is found in a single molecule study by van Oijen et al. (34). From low temperature measurements on LH1 and LH2, Pullerits et al. (20), Visser et al. (29), and Monshouwer et al. (35–37) established that the lowest exciton state is superradiant and delocalized over 2–3 pigments. Theoretical studies have established that the delocalization and energy transfer within the ring can be generally described using an exciton picture with a large amount of spectral disorder; i.e., the disordered exciton model (38–40). Such spectral disorder interferes with the possibility of a complete delocalization because it gives rise to nonuniform eigenfunctions. Dynamic disorder gives rise to extra coupling between the vibrational and exciton states (i.e., polaron formation) and thereby destroys the localization as well (40). Finally, it has been established that the transfer of electronic excitation within the exciton manifold includes a fast (fs) relaxation between exciton states within

Submitted September 11, 2010, and accepted for publication February 7, 2011.

*Correspondence: tacohenstuart@gmail.com

Editor: Leonid S. Brown.

0006-3495/11/05/2226/8 $2.00

doi: 10.1016/j.bpj.2011.02.048

strongly-coupled clusters and a slower (ps) energy migration between clusters or monomeric sites (3,39,41–44).

In our model, it is predicted that the dipole strength of the ring is mostly concentrated in three exciton states, $k = -1$, $k = 1$, and $k = 0$, delocalized over 7–11 molecules ($k = 1$, -1) and 2–4 molecules ($k = 0$) (45). A short pump-pulse excites a superposition of these one-exciton states, resulting in an excitonic wavepacket distributed over the circular structure with an effective width of ~4–5 molecules. This excited-state wavepacket exhibits a wavelike motion around the ring (for delocalized realizations of the disorder) or a hopping-type motion from one to another group of 3–5 molecules in a more localized (more-disordered) case (40). After the initial relaxation of the excited state, the 120-fs long dump pulse at 940 nm, such as the ones used in the experiments presented here, excites one or two vibronic levels states, typically creating a vibrational wavepacket in the $k = 0$, $k = 1$, or $k = -1$ exciton state. These vibrational wavepackets typically oscillate with 100–200 fs (20,26) (see the Supporting Material).

Because LH1 and LH2 have strong internal dipole coupling, exhibit fast transfer between the elements of the ring, and have a big absorption cross section and high structural stability, they make good candidates to study exciton interactions in photosynthesis. In this article, we utilize a pump-dump-probe technique to probe the excitonic and intraband dynamics in the transient absorption bands of LH1 (B875) and LH2 (B850). We elaborate on the reequilibration dynamics and the equilibration mechanism, and we discuss the advantages pump-dump-probe spectroscopy has to offer over regular pump-probe spectroscopy.

MATERIALS AND METHODS

Samples

The LH1-containing samples are membranes prepared from a mutant of *Rba. sphaeroides* lacking LH2, which therefore consists solely of RC-LH1-PufX complexes (46). These membranes, which contain dimeric core complexes, tend to form tubular structures due to the bend between the two halves of the dimer complex (13,47). The sample is dissolved in Tris:HCL (50 mM) and 0.1% lauryldimethylamine-oxide, to an optical density of ~0.7 at 880 nm. LH2 was purified from wild-type *Rba. sphaeroides* 2.4.1 (48) and dissolved in a Tris buffer of 20 mM and 0.1% lauryldimethylamine-oxide, to an optical density of ~0.6 at 800 nm.

Multipulse near infrared spectroscopy

The visible transient absorption experiments were performed on a so-called multipulse setup, special in its ability to produce two separately adjustable excitation pulses and a white-light continuum. Briefly, the output of a Ti:Sapphire regeneratively amplified laser system, operating at 1 kHz (Spitfire laser system; Spectra Physics, Irvine, CA) pumped with a 10 Watt Millennia continuous-wave pump laser (Spectra Physics), is divided into three beams. One beam was sent to a TOPAS (LightConversion, Vilnius, Lithuania) system to generate the excitation pulse at the desired center wavelengths of 795 or 895 nm; another was sent into a second TOPAS, set to produce the dump pulses of 895 or 940 nm. With the third beam, a white light continuum was generated by focusing on a translating 2-mm calcium fluorite plate. The excitation and dump pulse from the TOPAS were focused in the sample to a diameter of ~100 μm, and spatially overlapped with the probe beams.

The absorption changes were recorded, after being dispersed in a spectrograph, with a 256-element diode array (model No. S4801-256Q; Hamamatsu, Hamamatsu City, Japan). The pump and dump beam were set to a polarization of 54.7°, with respect to the probe beam with a Berek polarization compensator. The samples were put in a shaking 1-mm quartz cell. Two phase-locked choppers operating at 250 Hz and 125 Hz were used to ensure that the sample was excited by the pump-and-dump pulse and that reference spectra, where the sample is only probed by the white light continuum pulse, are recorded. The time delay among the pump, dump, and the probe beam was controlled by sending the dump-pulse and the probe beam over a variable optical delay line.

The instrument response function was determined via cross-correlation of the pump and probe and was ~120 fs. The pulses are measured by frequency-resolved optical gating and found to have a time-bandwidth product of 0.48–0.52, which is close to an ideal Gaussian (0.441). The pump pulses were set to be 10–20 nJ per pulse and the dump beam was set to 100–200 nJ per pulse. This difference is due the fact that we dump the very red wing of the excited state population. In addition, the pump-dump-probe (PDP) signal has low amplitude because only the doubly excited complexes generate the PDP signal. A complete scan averages 5000 pulses per time-point, and comprises a total of 110 time-points ranging from −10 ps to 7000 ps.

Pump-dump probe

In this article, we use the technique of pump-dump-probe (PDP) to perturb an existing excited-state population. The pump promotes the molecules to their excited state, and the following dump-pulse drives the population back into the ground state at a specific moment in time. The dump effectively stimulates emission to the ground state. By demoting a selective part of an excited-state manifold, the resulting perturbation of the equilibrium within that manifold can reveal the interaction between the states and the existence of otherwise hidden states (49). In these experiments, we record three different data sets: PDP, PP, and DP. These names refer to pump-dump-probe, pump-probe, and dump-probe, respectively. To visualize the effect of both the pump and the dump, we subtract the pump-probe and dump-probe data from the pump-dump-probe data and arrive at PDP minus PP minus DP (PDPmDPmPP). This procedure corrects the PDP data by removing the separate pump-probe and dump-probe dynamics from the pump-dump-probe dynamics.

RESULTS AND DISCUSSION

Steady-state spectroscopy

The steady-state absorption spectrum of the RC-LH1-PufX complexes shown in Fig. 1 (in *red*) consists mainly of a broad band at ~878 nm (B875) and two small bands at 770 nm and 800 nm belonging to the RC. The LH2 spectrum displays a two-band structure, representing the two BChl rings. The absorption at ~800 nm (B800) belongs to the ring with 9 BChls, and the 850 nm band (B850) belongs to the ring of 18 coupled BChls. In this experiment, we have chosen the pump wavelength for LH1 to be 895 nm, and the second pulse with which we demote the excited-state population is set to 940 nm. For LH2, the pump is set to 795 nm and the dump is set to 895 nm. The dump is chosen to demote as much of the excited-state population

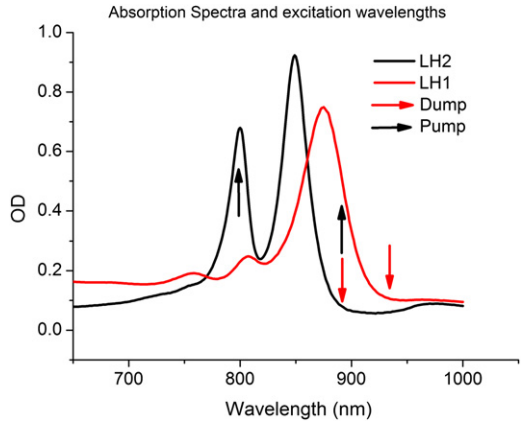

FIGURE 1 Absorption spectra of LH1 and LH2 of *Rba. sphaeroides*. The black and red arrows indicate the pump and dump frequencies used in the experiments. The dump is chosen to be in the very red wing of the absorption, to minimize effects due to repumping.

as possible while making sure it does not overlap with the absorption spectrum, to avoid repumping. Dump pulses centered at 895 nm and 940 nm for LH2 and LH1, respectively, were determined to be the most efficient for the purpose of these experiments.

Multipulse spectroscopy

Fig. 2 shows time-gated difference spectra generated upon pumping and dumping LH1. These spectra are constructed as follows. First, a pump pulse of the appropriate wavelength arrives at the sample (895 nm in the case of LH1). One picosecond after arrival of the pump pulse, a dump pulse arrives at the sample. As a reference, pump-probe spectra (recorded in the same measurement) have been added. This gives an idea about the efficiency of dumping the excited state and the amplitude of the exciton reequilibration process relative to the total absorption in such a measurement. Note that the times reported start from the dump moment ($T = 1$ ps). Fig. 2 essentially depicts the ultrafast reequilibration of the excitonic states at 905 nm and at 885 nm after a portion of the excited state has been dumped.

From the black spectrum to the magenta one, a buildup of amplitude is observed at ~905 nm during the first 200 fs. Up until 150 fs from time zero, the excitonic band at 885 nm stays almost at the same amplitude. After the excitonic states at 900 nm have been restored, a reequilibration of the 885-nm band still proceeds (*green* and *dark blue spectra*). The complete reequilibration to the new stable state takes ~500 fs, which is similar to previously reported equilibration times of 400–500 fs (20,24,50,51). Time traces of the dynamics of this reequilibration are displayed (see Fig. 4, later). (An apparent feature of the exciton bands at 885 and 905 nm is that they both blue-shift ~5 nm while they are thermally equilibrating. This blue shift is the result of a loss of the red-most states during the relaxation.) When the resultant spectra are closely inspected, an oscillatory feature superimposed on the equilibration of the two states is found and it appears that the dynamics of the equilibration of the two states at 885 nm and 905 nm is coupled. In the case of LH2, an excitation pulse at 795 nm is followed by a dump pulse at 895 nm arriving 5 ps later.

The time-gated difference spectra reported in Fig. 3 are from the moment that the dump-pulse arrives. At 5 ps, the bleaching signal due to the excited state is at the maximum amplitude and this makes it a good candidate for dumping

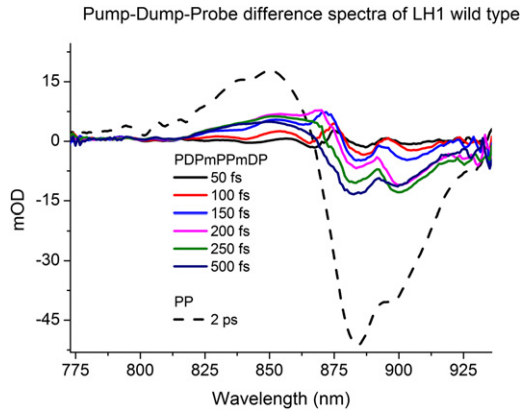

FIGURE 2 First, a pump pulse excites a population of the LH1 B875 band to its first excited state. The red wing of this state is then dumped by a resonant pulse at 940 nm. Selected early time-gated difference spectra show an ultrafast exciton reequilibration process of ~500 fs with an oscillatory component of ~150 fs. The pump-probe spectrum (*PP*) is added as a reference. The time reported is from the dump moment ($T = 1$ ps). *PDPmPPmDP* refers to the difference signal, pump-dump-probe minus pump-probe minus dump-probe, and *PP* refers to pump-probe.

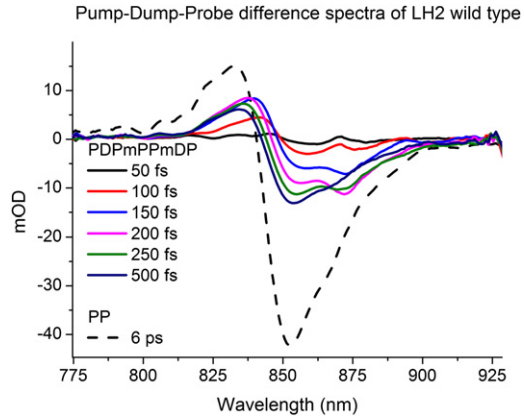

FIGURE 3 First, a pump pulse excites the population of the B800 band to the first excited state. The red wing of this state is then dumped by a resonant pulse at 895 nm. These time-gated difference spectra of LH2 show an ultrafast exciton reequilibration process of ~500 fs with an oscillatory component of ~150 fs. The pump-probe spectrum (*PP*) is added as a reference. The time reported is from the dump moment ($T = 5$ ps). *PDPmPPmDP* refers to the difference signal, pump-dump-probe minus pump-probe minus dump-probe, and *PP* refers to pump-probe.

its excited state. One can see the first black spectrum having a little positive band at ~870 nm. This hole is created by the dump-pulse. This hole is then refilled in 50–100 fs. We observe a similar behavior for the 850-nm band (the *red* and *blue spectrum*). The magenta and green spectra that follow show a growth around the bleach at 850 nm. This growth persists throughout for a total of 100–150 fs. Overall, it appears that when a dump-pulse demotes the excited-state population at ~895 nm, population of the exciton band at 870 nm is lost shortly afterwards.

There may be two origins of the 895 nm subband. First, it can be determined by a charge transfer state mixed with the exciton manifold, giving rise to a weakly allowed red state near 895 nm, so that a depopulation of this state is followed by a quick refilling from the 870 exciton state. The other possibility is that the 895-nm band corresponds to a dynamic vibrational hole created by the dump-pulse, which is later refilled via vibrational motion. In the last dark blue spectrum, the 850-nm and 870-nm exciton states are finally refilled to their equilibrium value. The timescale of this process (~400 fs) corroborates well with previously estimated numbers from measurements and modeling (24,50,52). A 5-nm blue shift of the exciton manifolds is also seen in the case of LH2. In Fig. 4, time traces of the dump-induced dynamics are depicted. The wavelength is chosen to be in the center of the exciton band.

After the perturbation by the dump-pulse, the manifold relaxes to its thermal equilibration according to relaxation-type dynamics. The exciton band at 870 nm is slowly refilled by the exciton band at 850 nm. The equilibration with even higher states ($k = +1, -1$) is ultrafast (10–50 fs), and has very small populations involved, making it impossible to observe these in our experiment. If the dynamics

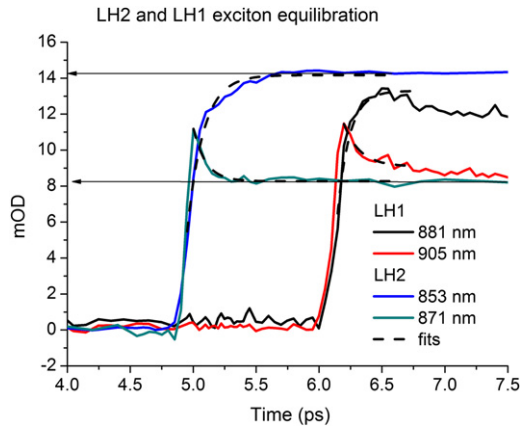

FIGURE 4 LH1 and LH2 kinetic traces for the different exciton bands. Depicted are the center frequencies of the exciton states in LH1 and LH2. The time traces show the behavior of the two main exciton bands after the dump arrived. Slight oscillatory features, which result from a vibrational wavepacket instigated by the dump pulse, overlay the traces during the first 500 fs after dumping. The LH1 traces are translated from 1 ps to 6 ps to depict their kinetics relative to LH2.

of equilibration of the excitonic bands in LH1 and LH2 (Figs. 2 and 3) are considered, a leading role for the α/β dimer over the ring structure has to be assumed. Although both antennas are ring-shaped, the LH1-sample is different from the LH2 in being a dimer. These LH1 dimers assume an S-shape, which can aggregate to form cylindrical metastructures (47,53–55). Apparently, an extended S-shaped LH structure does not strongly influence the exciton equilibration lifetime, because the exciton dynamics are very similar.

Although it has been stated in earlier single molecule measurements that the shape of the ring strongly governs the exciton states (56), such dependence cannot be found in the equilibration and vibrational dynamics presented here. From a molecular dynamics simulation on RC_LH1 rings and the RC_LH1_PufX complex, a similar observation was done. It was concluded that versus the normal circular shape, neither the S-shape, the bending, nor the structural discontinuity due to Puf-X significantly changes the exciton states involved in the dynamics (57). When the rise of the exciton band at 853 nm and the exciton band at 871 nm in LH2 are fitted with a single exponential, a comparable rate is found for both processes ($t = 0.13 \pm 0.01$ ps for the 871-nm band and 0.10 ± 0.01 ps for the 853 nm band), implying a coupling of the equilibration process of both states. Similar rates are also found for the LH1 complex. Note that the rise and decay are calculated from 4.95 ps, where they overlap (Fig. 4). The amplitude of the equilibration feature of the 853-nm exciton band is ~2–3 times larger than the 871-nm exciton band during the first 200 fs. This corresponds to the difference in delocalization (or radiative rate) between $k = 0$ and $k = 1$, which is consistent with the proposed disordered-exciton model.

Oscillatory features superimposed onto the exciton equilibration due to a vibrational wavepackets can be observed in Fig. 4. This feature is shown by taking the residuals (raw data minus exponential fit; see Fig. 5). The oscillatory features of the two exciton bands show a coupled phase behavior (in other words, they are in phase), and a fast Fourier transform of the oscillations results in peak amplitude at a frequency of 6 per picosecond, or a wavepacket period of ~165 fs. The disordered-exciton model predicts that the superposition of one-exciton states created by the pump pulse shows a coherent equilibration. This coherence is found in the phase behavior of the vibrational wavepacket created by the dump pulse. After 400–500 fs, when the equilibration is over, this phase-correlation is lost. Similar behavior is found for LH1, but the results are less pronounced.

Pump-probe measurements on the B850 band of the LH2 complex of *Rhodopseudomonas palustris* have estimated an exciton-state relaxation lifetime between 500 and 650 fs (58). An extensive quantitative theoretical description of these reequilibration dynamics is found in Novoderezhkin et al. (61).

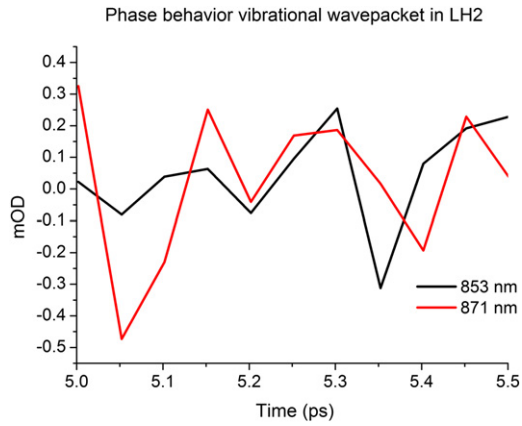

FIGURE 5 The two exciton bands at 853 nm and 871 nm both show an oscillatory component in their equilibration dynamics. The oscillatory feature superimposed on the exciton equilibration as seen in Fig. 4, are presented here for LH2. This picture is produced by subtracting the single exponential fit from the raw data in Fig. 4. The resulting oscillatory feature represents a vibrational wavepacket created by the dump pulse. Plotting the feature for the two exciton bands shows that their wavepacket is in phase for the duration of the equilibration (until 5.35 ps).

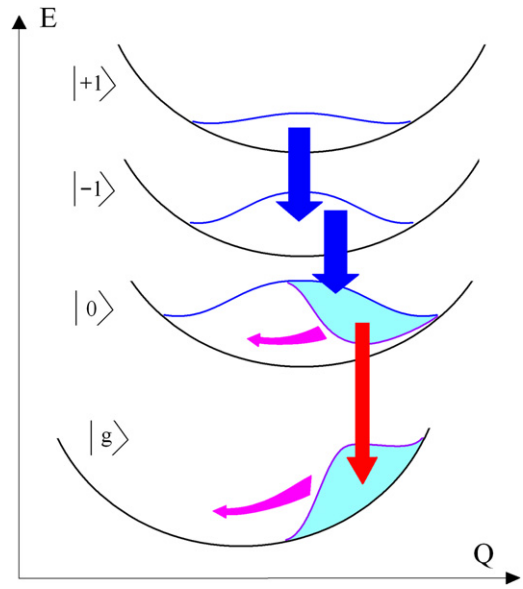

FIGURE 6 Exciton energy diagram illustrating the dynamics of pump-dump-probe response. Potential energy E as a function of an effective nuclear coordinate Q is shown for the ground (g), and three lowest exciton states ($k = 0, -1, 1$) of the circular aggregate. Blue arrows indicate ultrafast exciton equilibration from higher exciton states (not seen in this experiment) and the red arrow indicates the equilibration between $k = 0$ and $k = 1$. Magenta arrows indicate the vibrational wavepacket motion, in phase, imposed on this equilibration, from $k = 1$ to $k = 0$. (This picture is taken from Novoderezhkin et al. (61).)

CONCLUSIONS

In this work, we have applied pump-dump-probe spectroscopy to investigate the dynamics of the lower exciton state of the bacterial light-harvesting complexes LH1 and LH2. A schematic picture illustrating the dynamics observed in our PDP measurement is shown in Fig. 6. The first pump-pulse creates an excited-state wavepacket (superposition of the one-exciton states) that is subsequently (after excited-state equilibrium is reached) perturbed by a second dump-pulse transferring some part of the population back to the ground state. The subsequent reequilibration is then monitored by the third probe pulse. The dump pulse depopulates the lowest $k = 0$ level without repumping of the excited states via ground-state absorption and without population of the two-exciton states via excited-state absorption. This is possible by tuning the dump wavelength to the red, where the pulse spectrum is well overlapped with stimulated emission of the lowest state and does not overlap with the ground- and excited-state absorption.

Vibrational wavepackets associated with the three lowest exciton states and corresponding to exciton-vibrational equilibration (reached at several picoseconds after impulsive excitation) are shown by the blue lines in Fig. 6. Their integrated areas and shapes reflect the Boltzmann distribution of the excitation density over the exciton states and over the vibrational sublevels, respectively. The action of the dump pulse tuned to the long-wavelength side of the absorption band (*red arrow*) creates a hole in the steady-state vibrational wavefunction of the lowest ($k = 0$) exciton level (*cyan area*), moving some part of the nuclear wavepacket to the ground state (*cyan*). The spectral width of the 120-fs dump pulse is not enough to interact with the higher ($k = -1$) level whereas a spectrally broader dump pulse can, in principle, depopulate the ($k = -1$) level as well and create some coherence between ($k = 0$) and ($k = -1$). Such selective depopulation of the ($k = 0$) level produces more pronounced reequilibration between the three lowest exciton states via exciton relaxation from the higher levels (*blue arrows*).

On the other hand, a dump of the excited state creates a vibrational coherence in both the ($k = 0$) exciton state and ground state. A subsequent coherent motion of the excited-state hole and ground-state wavepackets (*cyan arrows*) gives rise to oscillations of the stimulated emission (at ~870 nm in the case of B850 ring) and photobleaching band (peaking at 850 nm for B850). These oscillations should be in-phase (as was shown in Novoderezhkin et al. (40,52)). Note that this is in agreement with the 850- and 870-nm kinetics shown in Fig. 4 (see oscillatory features between 5.1 and 5.7 ps for LH2). It is also remarkable that the absorption changes after the dump are several times bigger for the 850-nm than for the 870-nm region. This reflects the fact that the dipole strength of the ($k = -1, 1$) band is 5–6 times larger than for the ($k = 0$) band, so that any exchange in excitation density between these bands will produce a corresponding spectral response with nonequal amplitudes.

The pump-dump-probe measurements on the LH1 and LH2 antennae of *Rba. sphaeroides* have allowed us to

visualize, directly, the reequilibration of the excitonic states and vibrational wavepackets created by the dump pulse. The spectral resolution these pump-dump-probe data provide leads us to conclude that our multipulse spectroscopy approach is valid for studying excitonic interaction and vibrational relaxation in such coupled systems.

In conventional pump-probe, a relaxation is observed upon excitation of higher exciton states, that are 1), only weakly allowed; 2), very fast (<20 fs) decaying; and 3), superimposed on the intense vibrational wings of the lower superradiant levels. Thus, excitation of higher levels is never selective, and the fast downhill transfers from higher levels typically are hidden under the pump-pulse envelope and coherent artifacts (59). Excitation of the ($k = -1$, 1) levels near the absorption maximum is not selective either. It is accompanied by population of the lowest level through its vibrational wing and via fast relaxation from ($k = -2$, 2) levels. The latter are superimposed on the ($k = -1$, 1) band and have significantly faster relaxation compared to the ($k = 0$) level (59,60). The relaxation-induced red-shift of transient absorption in this case is less pronounced than for blue excitation, so that relaxation dynamics are difficult to extract from the background (i.e., strong ground-state bleaching that can exhibit its own dynamics due to vibrational coherences and relaxation).

In pump-dump-probe, the relaxation dynamics are much better resolved due to the selective interaction of the dump with only one level. In addition, we selectively monitor the relaxation between the three lowest levels, as relaxation from short-lived higher ($k = 2$, 3, and higher) levels is excluded because they are not populated in equilibrium. The spectral changes with which the relaxation processes between ($k = -1$, 1) and ($k = 0$) levels occur have relatively large amplitudes because these levels are superradiant (37). Using a two-pulse technique, therefore, increases the relative spectral resolution of the exciton levels when compared to a one-pulse technique. Because the relaxation between ($k = -1$, 1) and ($k = 0$) levels is slower then the relaxation from higher ($k = 2$, 3) levels, these experiments allow us to study these separately. This allows for a greater understanding of the excited-state relaxation. The lifetime found for the equilibration process in LH1 and LH2 (400–500 fs) is in accordance with previously measured and calculated values, as is the oscillatory component of ~165 fs.

Both these observations are predicted from the disordered-exciton model proposed and used to describe LH1 and LH2 (40,45,52,59). At the moment, two models exist for the spectroscopy and exciton dynamics of the LH2-B850 antenna emerging from the interpretation of the bulk nonlinear spectra and single molecule data—the disordered-exciton model and the model with elliptical deformation implying correlated disorder in combination with a little amount of uncorrelated disorder. Modeling of the PDP data gives strong support for the disordered-exciton model. The key properties of this model are:

1. The existence of a strongly allowed (superradiant) lowest $k = 0$ exciton level (in contrast to elliptical model, where the $k = 0$ level is only weakly allowed);

2. Big variation of the exciton wavefunctions (including their delocalization and overlap) producing big spread of relaxation rates in different realizations of the disorder.

The consistent and quantitative explanation of the spectra and nonlinear kinetics as performed in Novoderezhkin et al. (61) enables us to extract reliable information about some specific features of the excitation dynamics in the LH2 complex. The first remarkable fact is the possibility of a selective excitation of the lowest exciton state at 895 nm. This is only possible if the $k = 0$ emission profile is (much) more intense than the wings of the emission spectra from the higher levels. Our modeling demonstrates that the initial conditions (population changes induced by the dump) cannot be reproduced if the $k = 0$ level is not superradiant on average.

The superradiant character of the lowest level is further corroborated by the ratio of the amplitudes of the 870- and 850-nm PDP signals. We demonstrated that the observed ratio can be reproduced by the disordered model with the ratio of the dipole strengths of $D_2/D_1 = 6.02/2.57 = 2.34$ (the apparent ratio of the PDP amplitudes generally is not identical to dipole strengths ratio, but in our case it is close, i.e., 2.75). The dipole strength of the lowest level extracted from the fit, i.e., $D_1 = 2.57$, is in excellent agreement with the superradiant experiment (37) giving the value of 2.8.

Finally, our modeling of the PDP-experiments confirms the existence of realizations with a localized and red-shifted $k = 0$ level. These realizations give rise to the enormous spread of the relaxation rates, yielding slow components in the relaxation between the lowest states, experimentally observed as slow components in the PDP kinetics. In conclusion, our study demonstrates that the multipulse technique (in particular, pump-dump-probe) is a powerful tool for exploring the equilibration dynamics within the excited-state manifold, giving what we believe to be a unique possibility to highlight any particular relaxation channel and property of individual excited states. In combination with conventional spectroscopy methods, this allows a more precise estimation of the key parameters that determine the whole energy transfer event.

SUPPORTING MATERIAL

Three figures are available at http://www.biophysj.org/biophysj/supplemental/S0006-3495(11)00299-2.

This research was supported by The Netherlands Organization for Scientific Research through the Dutch Foundation for Earth and Life Sciences (investment grant No. 834-01-002) and funding from the European Commission's Seventh Framework Program (LASERLAB-EUROPE, grant agreement No. 228334, Project ID: VULRC001507). T.A.C.S. received support from the Netherlands Organization for Scientific Research, Chemical Sciences

(NWO-CW grant No. 700-53-307). R.J.C. and C.N.H. were supported by the Biotechnology and Biological Sciences Research Council, and as part of the Photosynthetic Antenna Research Center, an Energy Frontier Research Center funded by the U.S. Department of Energy, Office of Science, Office of Basic Energy Sciences under award No. DE-SC 0001035.

REFERENCES

1. Somsen, O. J. G., F. van Mourik, …, L. Valkunas. 1994. Energy migration and trapping in a spectrally and spatially inhomogeneous light-harvesting antenna. *Biophys. J.* 66:1580–1596.
2. Sundstrom, V., T. Pullerits, and R. van Grondelle. 1999. Photosynthetic light-harvesting: reconciling dynamics and structure of purple bacterial LH2 reveals function of photosynthetic unit. *J. Phys. Chem. B.* 103:2327–2346.
3. Novoderezhkin, V. I., D. Rutkauskas, and R. van Grondelle. 2006. Dynamics of the emission spectrum of a single LH2 complex: interplay of slow and fast nuclear motions. *Biophys. J.* 90:2890–2902.
4. Roszak, A. W., T. D. Howard, …, R. J. Cogdell. 2003. Crystal structure of the RC-LH1 core complex from *Rhodopseudomonas palustris*. *Science.* 302:1969–1972.
5. Jamieson, S. J., P. Wang, …, P. A. Bullough. 2002. Projection structure of the photosynthetic reaction center-antenna complex of *Rhodospirillum rubrum* at 8.5 Å resolution. *EMBO J.* 21:3927–3935.
6. McDermott, G., S. M. Prince, …, N. W. Isaacs. 1995. Crystal structure of an integral membrane light-harvesting complex from photosynthetic bacteria. *Nature.* 374:517–521.
7. Olsen, J. D., J. N. Sturgis, …, B. Robert. 1997. Site-directed modification of the ligands to the bacteriochlorophylls of the light-harvesting LH1 and LH2 complexes of *Rhodobacter sphaeroides*. *Biochemistry.* 36:12625–12632.
8. Walz, T., S. J. Jamieson, …, C. N. Hunter. 1998. Projection structures of three photosynthetic complexes from *Rhodobacter sphaeroides*: LH2 at 6 Å, LH1 and RC-LH1 at 25 Å. *J. Mol. Biol.* 282:833–845.
9. Lilburn, T. G., C. E. Haith, …, J. T. Beatty. 1992. Pleiotropic effects of PufX gene deletion on the structure and function of the photosynthetic apparatus of *Rhodobacter capsulatus*. *Biochim. Biophys. Acta.* 1100:160–170.
10. Qian, P., C. N. Hunter, and P. A. Bullough. 2005. The 8.5Å projection structure of the core RC-LH1-PufX dimer of *Rhodobacter sphaeroides*. *J. Mol. Biol.* 349:948–960.
11. Barz, W. P., A. Verméglio, …, D. Oesterhelt. 1995. Role of the PufX protein in photosynthetic growth of *Rhodobacter sphaeroides*. 2. PufX is required for efficient ubiquinone/ubiquinol exchange between the reaction center QB site and the cytochrome bc1 complex. *Biochemistry.* 34:15248–15258.
12. McGlynn, P., C. N. Hunter, and M. R. Jones. 1994. The *Rhodobacter sphaeroides* PufX protein is not required for photosynthetic competence in the absence of a light harvesting system. *FEBS Lett.* 349:349–353.
13. Qian, P., P. A. Bullough, and C. N. Hunter. 2008. Three-dimensional reconstruction of a membrane-bending complex: the RC-LH1-PufX core dimer of *Rhodobacter sphaeroides*. *J. Biol. Chem.* 283:14002–14011.
14. Trautman, J. K., A. P. Shreve, …, A. C. Albrecht. 1990. Femtosecond dynamics of energy transfer in B800-850 light-harvesting complexes of *Rhodobacter sphaeroides*. *Proc. Natl. Acad. Sci. USA.* 87:215–219.
15. Deisenhofer, J., O. Epp, …, H. Michel. 1985. Structure of the protein subunits in the photosynthetic reaction center of *Rhodopseudomonas viridis* at 3 Å resolution. *Nature.* 318:618–624.
16. Nagarajan, V., E. T. Johnson, …, W. W. Parson. 1999. Femtosecond pump-probe spectroscopy of the B850 antenna complex of *Rhodobacter sphaeroides* at room temperature. *J. Phys. Chem. B.* 103: 2297–2309.
17. Guo, L. J., Y. Liu, …, S. Qian. 2002. The observation of excited-state dynamical evolution in light-harvesting complex LH2 from *Rhodobacter sphaeroides* 601. *FEBS Lett.* 511:69–72.
18. Rätsep, M., C. N. Hunter, …, A. Freiberg. 2005. Band structure and local dynamics of excitons in bacterial light-harvesting complexes revealed by spectrally selective spectroscopy. *Photosynth. Res.* 86:37–48.
19. Timpmann, K., G. Trinkunas, …, A. Freiberg. 2005. Excitons in core LH1 antenna complexes of photosynthetic bacteria: evidence for strong resonant coupling and off-diagonal disorder. *Chem. Phys. Lett.* 414:359–363.
20. Pullerits, T., M. Chachisvalis, …, V. Sundström. 1994. Exciton dynamics in the light-harvesting complexes of *Rhodobacter sphaeroides*. *Chem. Phys. Lett.* 224:355–365.
21. Koolhaus, M. H., R. N. Frese, …, R. van Grondelle. 1998. Identification of the upper exciton component of the B850 bacteriochlorophylls of the LH2 antenna complex, using a B800-free mutant of *Rhodobacter sphaeroides*. *Biochemistry.* 37:4693–4698.
22. Salverda, J. M., F. van Mourik, …, R. van Grondelle. 2000. Energy transfer in the B800 rings of the peripheral bacterial light-harvesting complexes of *Rhodopseudomonas acidophila* and *Rhodospirillum molischianum* studied with photon echo techniques. *J. Phys. Chem. B.* 104:11395–11408.
23. Visser, H. M., O. J. Somsen, …, R. van Grondelle. 1995. Direct observation of sub-picosecond equilibration of excitation energy in the light-harvesting antenna of *Rhodospirillum rubrum*. *Biophys. J.* 69:1083–1099.
24. De Caro, C., R. W. Visschers, …, S. Voelker. 1994. Inter- and intraband energy transfer in LH2-antenna complexes of purple bacteria. A fluorescence line-narrowing and hole-burning study. *J. Phys. Chem.* 98:10584–10590.
25. Nagarajan, V., R. G. Alden, …, W. W. Parson. 1996. Ultrafast exciton relaxation in the B850 antenna complex of *Rhodobacter sphaeroides*. *Proc. Natl. Acad. Sci. USA.* 93:13774–13779.
26. Chachisvilis, M., Oliver Kühn, …, V. Sundström. 1997. Excitons in photosynthetic purple bacteria: wavelike motion or incoherent hopping? *J. Phys. Chem. B.* 101:7275–7283.
27. Book, L. D., A. E. Ostafin, …, N. F. Scherer. 2000. Exciton delocalization and initial dephasing dynamics of purple bacterial LH2. *J. Phys. Chem. B.* 104:8295–8307.
28. Polivka, T., T. Pullerits, …, V. Sundström. 2000. Exciton relaxation and polaron formation in LH2 at low temperature. *J. Phys. Chem. B.* 104:1088–1096.
29. Visser, H. M., O. J. G. Somsen, …, R. van Grondelle. 1996. Excited-state energy equilibration via subpicosecond energy transfer within the inhomogeneously broadened light-harvesting antenna of LH-1-only *Rhodobacter sphaeroides* mutants M2192 at room temperature and 4.2 K. *J. Phys. Chem.* 100:18859–18867.
30. Bradforth, S. E., R. Jimenez, …, G. R. Fleming. 1995. Excitation transfer in the core light harvesting complex (LH-1) of *Rhodobacter sphaeroides*: an ultrafast fluorescence depolarization and annihilation study. *J. Phys. Chem.* 99:16179–16191.
31. Jimenez, R., S. N. Dikshit, …, G. R. Fleming. 1996. Electronic excitation transfer in the LH2 complex of *Rhodobacter sphaeroides*. *J. Phys. Chem.* 100:6825–6834.
32. Tretiak, S., D. Middleton, …, S. Mukamel. 2000. Bacteriochlorophyll and carotenoid excitonic couplings in the LH2 system of purple bacteria. *J. Phys. Chem. B.* 104:9540–9553.
33. Krueger, B. P., G. D. Scholes, and G. R. Fleming. 1998. Calculation of couplings and energy-transfer pathways between the pigments of LH2 by the ab initio transition density cube method. *J. Phys. Chem. B.* 102:5378–5386.
34. Van Oijen, A., M. Ketelaars, …, J. Schmidt. 1999. Unraveling the electronic structure of individual photosynthetic pigment-protein complexes. *Science.* 285:400–402.
35. Monshouwer, R., I. O. De Zarate, …, R. van Grondelle. 1995. Low intensity pump-probe spectroscopy on the B800 to B850 transfer in

the light harvesting 2 complex of *Rhodobacter sphaeroides*. *Chem. Phys. Lett.* 246:341–346.

36. Monshouwer, R., A. Baltuška, …, R. van Grondelle. 1998. Time-resolved absorption difference spectroscopy of the LH-1 antenna of *Rhodopseudomonas viridis*. *J. Phys. Chem. A.* 102:4360–4371.
37. Monshouwer, R., M. Abrahamsson, …, R. van Grondelle. 1997. Superradiance and exciton delocalization in bacterial photosynthetic light-harvesting systems. *J. Phys. Chem. B.* 101:7241–7248.
38. Alden, R. G., E. Johnson, …, R. J. C. Cogdell. 1997. Calculations of spectroscopic properties of the LH2 bacteriochlorophyll-protein antenna complex from *Rhodopseudomonas acidophila*. *J. Phys. Chem. B.* 101:4667–4680.
39. Zigmantas, D., E. L. Read, …, G. R. Fleming. 2006. Two-dimensional electronic spectroscopy of the B800-B820 light-harvesting complex. *Proc. Natl. Acad. Sci. USA*. 103:12672–12677.
40. Novoderezhkin, V., R. Monshouwer, and R. van Grondelle. 1999. Disordered exciton model for the core light-harvesting antenna of *Rhodopseudomonas viridis*. *Biophys. J.* 77:666–681.
41. van Grondelle, R., and V. I. Novoderezhkin. 2005. Energy transfer in photosynthesis: experimental insights and quantitative models. *Phys. Chem. Chem. Phys.* 8:793–807.
42. Beekman, L. M. P., M. Steffen, …, R. van Grondelle. 1997. Characterization of the light-harvesting antennas of photosynthetic purple bacteria by stark spectroscopy. 1. LH1 antenna complex and the B820 subunit from *Rhodospirillum rubrum*. *J. Phys. Chem. B.* 101: 7284–7292.
43. Beekman, L. M. P., R. N. Frese, …, R. van Grondelle. 1997. Characterization of the light-harvesting antennas of photosynthetic purple bacteria by Stark spectroscopy. 2. LH2 complexes: influence of the protein environment. *J. Phys. Chem. B.* 101:7293–7301.
44. Mukai, K., and S. Abe. 2001. Effects of positional disorder on optical absorption spectra of light-harvesting antenna complexes in photosynthetic bacteria. *Chem. Phys. Lett.* 336:445–450.
45. Novoderezhkin, V., M. Wendling, and R. van Grondelle. 2003. Intra- and interband transfers in the B800–B850 antenna of *Rhodospirillum molischianum*: Redfield theory modeling of polarized pump-probe kinetics. *J. Phys. Chem. B.* 107:11534–11548.
46. Jones, M. R., G. J. Fowler, …, C. N. Hunter. 1992. Mutants of *Rhodobacter sphaeroides* lacking one or more pigment-protein complexes and complementation with reaction-center, LH1, and LH2 genes. *Mol. Microbiol.* 6:1173–1184.
47. Frese, R. N., J. D. Olsen, …, R. van Grondelle. 2000. The long-range supraorganization of the bacterial photosynthetic unit: a key role for PufX. *Proc. Natl. Acad. Sci. USA*. 97:5197–5202.
48. Hawthornethwaite-Lawless, A. M., and R. J. Cogdell. 1991. Bacteriochlorophyll-binding proteins. *In* The Chlorophylls. H. Scheer, editor. CRC Press, Boca Raton, FL. 493–528.
49. Cohen Stuart, T. A., and R. van Grondelle. 2009. Multipulse spectroscopy on the wild-type and YM210W bacterial reaction center uncovers a new intermediate state in the special pair excited state. *Chem. Phys. Lett.* 474:352–356.
50. Freiberg, A., K. Timpmann, …, N. W. Woodbury. 1998. Exciton relaxation and transfer in the LH2 antenna network of photosynthetic bacteria. *J. Phys. Chem. B.* 102:10974–10982.
51. Haran, G., K. Wynne, …, R. M. Hochstrasser. 1996. Level mixing and energy redistribution in bacterial photosynthetic reaction centers. *J. Phys. Chem.* 100:5562–5569.
52. Novoderezhkin, V., R. Monshouwer, and R. van Grondelle. 1999. Exciton (de)localization in the LH2 antenna of *Rhodobacter sphaeroides* as revealed by relative difference absorption measurements of the LH2 antenna and the B820 subunit. *J. Phys. Chem. B.* 103:10540–10548.
53. Hsin, J., J. Gumbart, …, K. Schulten. 2009. Protein-induced membrane curvature investigated through molecular dynamics flexible fitting. *Biophys. J.* 97:321–329.
54. Siebert, C. A., P. Qian, …, P. A. Bullough. 2004. Molecular architecture of photosynthetic membranes in *Rhodobacter sphaeroides*: the role of PufX. *EMBO J.* 23:690–700.
55. Jungas, C., J. L. Ranck, …, A. Verméglio. 1999. Supramolecular organization of the photosynthetic apparatus of *Rhodobacter sphaeroides*. *EMBO J.* 18:534–542.
56. Oellerich, S., and J. Köhler. 2009. Low-temperature single-molecule spectroscopy on photosynthetic pigment-protein complexes from purple bacteria. *Photosynth. Res.* 101:171–179.
57. Sener, M., J. Hsin, …, K. Schulten. 2009. Structural model and excitonic properties of the dimeric RC-LH1-PufX complex from *Rhodobacter sphaeroides*. *Chem. Phys.* 357:188–197.
58. Moulisová, V., L. Luer, …, R. J. Cogdell. 2009. Low light adaptation: energy transfer processes in different types of light harvesting complexes from *Rhodopseudomonas palustris*. *Biophys. J.* 97:3019–3028.
59. van Grondelle, R., and V. Novoderezhkin. 2001. Dynamics of excitation energy transfer in the LH1 and LH2 light-harvesting complexes of photosynthetic bacteria. *Biochemistry.* 40:15057–15068.
60. Kuhn, O., and V. Sundstrom. 1997. Pump-probe spectroscopy of dissipative energy transfer dynamics in photosynthetic antenna complexes: a density matrix approach. *J. Chem. Phys.* 107:4154–4164.
61. Novoderezhkin, V. I., T. A. Cohen Stuart, and R. van Grondelle. 2011. Dynamics of exciton relaxation in LH2 antenna probed by multipulse nonlinear spectroscopy. *J. Phys. Chem. A*. 10.1021/jp108187m.